REALISTIC WIND LOADING ON UNREINFORCED MASONRY WALLS

A. Udey[1] and B.F. Sparling[2]
[1] Master of Science Student, Department of Civil and Geological Engineering, University of Saskatchewan, Saskatoon, SK, S7N 5A9, Canada, a.udey@usask.ca
[2] Professor, Department of Civil and Geological Engineering, University of Saskatchewan, Saskatoon, SK, S7N 5A9, Canada, bruce.sparling@usask.ca

ABSTRACT
Twenty full-scale masonry walls were constructed and tested to failure in the Structures Laboratory at the University of Saskatchewan. One half of the specimens were loaded laterally with monotonically increasing quasi-static loads that reproduced the effects of a uniform wind pressure, while the remainder were loaded with dynamic time histories that varied randomly in a manner similar to gusty winds. Additionally, one half of the specimens within both loading regimes were constructed with true pinned connections at their top and bottom ends, while the other half of the wall specimens featured support conditions similar to nominally "pinned" supports typically encountered in practice. The research was done to determine the influence of load and connection type on the behavior of the masonry walls. It was found that walls constructed with more realistic support conditions exhibited both substantially higher bending moment resistance and greater ductility. Walls with realistic supports that were subjected to dynamic loading resembling natural wind sustained slightly higher peak moments and exhibited larger lateral displacements at failure than companion statically loaded specimens. In all cases, though, failure seemed to be initiated when a geometrically unstable displaced shape was attained. In the dynamic load tests, failure generally occurred during a sustained, large amplitude "gust", rather than necessarily at the highest instantaneous peak load within the loading history.

KEYWORDS: masonry walls, wind loading, support conditions, unreinforced, lateral loading

INTRODUCTION
There is currently little research relating to the influence of dynamic wind loading on masonry structures. Research concerned with out-of-plane dynamic loading of masonry walls has primarily been focused on enforced support movement, replicating earthquake loads [1], or on blast loading [2]. Masonry research dealing with wind has generally been targeted at information regarding roof and building cladding performance [3]. As a result, there is a gap in the knowledge base regarding the effects of realistic wind on structural masonry walls.

Natural wind within the atmospheric boundary layer may be described as a moving air mass containing turbulent vortices of varying sizes, ranging from several hundred meters to less than a meter in extent, travelling at different velocities. As a result, the wind speed observed at a given location will vary randomly with time, but can be separated into two components: a steady (time-invariant) mean wind speed, and dynamic gusts of varying durations that fluctuate randomly about the mean value. For design purposes, wind loads are normally characterized by static pressure distributions defined in terms of a specified mean pressure that is increased by a "gust factor" to account for increases in wind speed to due turbulence [4]. Such an approach

inherently assumes that the structure responds in a quasi-static manner to the peak gust, with no differentiation between the effects of steady and dynamically varying applied forces. However, that assumption may be questionable for relatively massive structures like masonry walls for which inertia may play a significant role. To date, though, research relating to wind-like flexural loading of masonry walls has been exclusively focused on quasi-static behaviour.

Similarly, flexural tests of masonry walls have typically been carried out using idealized pinned supports to permit an accurate characterization of end restraint conditions [5,6]. For simplicity, the assumption of pinned end conditions is also routinely made in the design and analysis of masonry walls. In practice, though, wall supports inevitably provide some degree of rotational restraint arising from the finite thickness of the masonry units and the nature of common construction details. It can be expected, then, that the added stiffness of the support can provide reserve strength to the wall that is generally unaccounted for in design.

RESEARCH OBJECTIVES

An experimental research program was undertaken to investigate the behaviour of unreinforced concrete block masonry walls under out-of-plane loading applied both statically and dynamically, as well as to study the influence of end support restraint. More specifically, the research objectives were:

- To compare the strength and behaviour of masonry walls subjected to monotonically increasing quasi-static loads representative of steady uniform wind pressures versus dynamic force time histories that varied over time in a manner similar to gusty wind; and
- To determine the differences in behaviour between unreinforced masonry walls with ideal pinned supports, representing conditions commonly assumed in analysis and design, and realistic end support connections that are typically encountered in the field.

DESCRIPTION OF THE EXPERIMENTAL PROGRAM

Twenty unreinforced and ungrouted masonry wall specimens were constructed between September 28 and October 6, 2011 in the Structural Laboratory at the University of Saskatchewan by a qualified mason. Each masonry wall was 15 courses (3.0 m) tall and 2.5 blocks (1.0 m) wide, and was built in running bond using standard 200 mm hollow concrete masonry blocks with a nominal compressive strength of 15 MPa and Type S mortar conforming to the requirements of CSA Standard A179 [7]. Three course high masonry prisms, along with bond wrench test specimens and standard mortar cubes, were also constructed and tested.

As illustrated in Figure 1, two types of specimens were constructed (ten specimens of each type), differing only in the support details at the top and bottom of the walls. Specimens designated as having “ideal” pinned supports were constructed on a steel base plate that, during testing, was placed on a knife-edge support aligned with the centre of the specimen. The top support for the “ideal” case consisted of a steel plate clamped to the top of the wall which was supported laterally by three horizontal steel rods that were pin-connected to the top plate on one end and to a rigid reaction frame on the other.

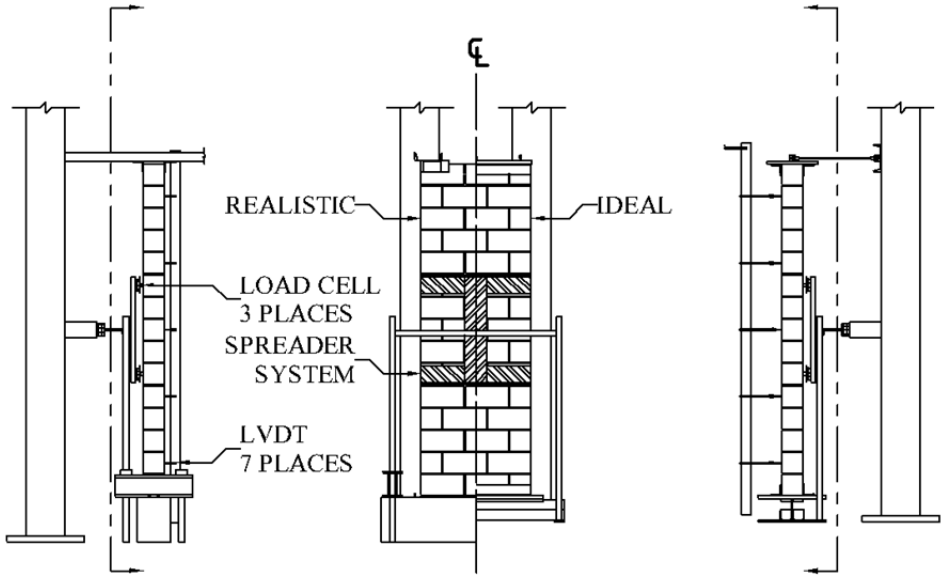

Figure 1: Apparatus for wall tests

Specimens designated as having "realistic" pinned supports were constructed and tested on concrete beams secured to the laboratory strong-floor, with a 10 mm mortar joint between the concrete beam and the face shell of the first course of block to simulate typical field construction practices. The top support for the "realistic" case was provided by four 150 mm long guide angles, with one angle placed at either end of the specimen on both faces; the guide angles were brought into contact with the face of the wall to prevent transverse displacements at those locations, but were not clamped or secured to the wall in any manner. The guide angles were attached to a horizontal support beam above the wall specimen that was positioned such that there was a vertical gap between the specimen and the support beam to ensure that no contact occurred during testing.

The wall specimens were divided into four test series, with five specimens in each series: specimens with "ideal" pinned supports tested under quasi-static loading (denoted as IS); specimens with "ideal" pinned supports tested under dynamic loading (denoted as ID); specimens with "realistic" pinned supports tested under quasi-static loading (denoted as RS); and specimens with "realistic" pinned supports tested under dynamic loading (denoted as RD). All of the wall specimens were tested in the same loading frame, a schematic of which is shown in Figure 1. The left side of the schematic depicts the test setup for the realistically pinned walls, while the right side shows the setup for the ideally pinned walls.

Loading was applied to the walls using the hydraulic actuator shown in Figure 2, which was oriented horizontally and positioned at the centre of the wall. Four-point loading was generated using a spreader system to split the load between two levels separated by a vertical distance of 800 mm; these applied loads were then spread horizontally across the width of the wall as shown in Figure 3. Care was taken to ensure that all loading and reaction points functioned as frictionless pins so that the load spreader system was statically determinate.

A load cell placed between the actuator and vertical spreader beam was used to measure the total applied load, while two additional load cells were placed between the spreader beam and the wall to measure the loads applied to the wall at both loading levels. A linearly variable differential transducer (LVDT) attached to the hydraulic actuator (Figure 3) measured horizontal displacements at the loading point. Seven additional LVDT's were distributed along the vertical and horizontal centre lines of the wall (see Figure 1) on the unloaded face to better define the deflected shape of the specimen; these LVDT's were removed well before collapse of the wall to avoid damage to the instrumentation.

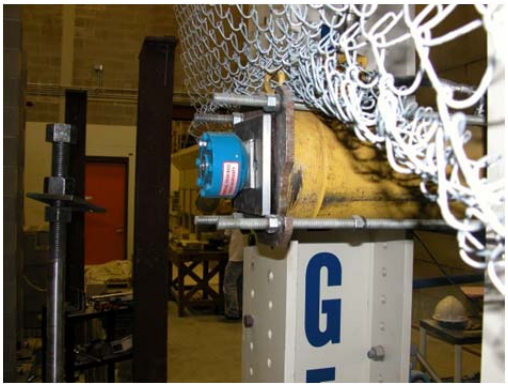

Figure 2: Hydraulic actuator

Figure 3: LVDT and Spreader system

The data was collected using LabView™ software implemented on a 16-bit data acquisition system featuring an NI PCI-6024E data acquisition card and a model SCXI-1001 chassis from National Instruments™. Data was sampled at rates ranging from 16 to 20 Hz and stored electronically for subsequent processing.

For the quasi-static loading test series, the actuator was run under displacement control at a rate of 3 mm/min in order to obtain a good definition of post-cracking behaviour. Dynamic load tests, on the other hand, were run under load control in an attempt to better simulate natural wind loading. A description of the dynamic loading is provided in the following section.

WIND LOAD GENERATION

Random dynamic loading time histories were generated based on simulated wind speed records that reproduced the essential temporal characteristics of gusty winds. For this purpose, the wind time histories were mathematically generated using a 4th order autoregressive process [8], based on a formulation described in [9]. Wind conditions were modelled for a fictitious point located at an elevation of 10 m above the ground on what could be characterized as "rough terrain" [4].

Each simulated wind speed time history represented a 10 min duration wind storm defined at 0.05 s increments. The wind speed (V) time histories were converted to dynamic wind pressures (q) according to the relationship:

$$q = \frac{1}{2}\rho V^2 \qquad [1]$$

where ρ is the mass density of air (1.29 kg/m^3), and finally to force time histories by assuming fully correlated wind pressures over a tributary area of 3.0 m^2. Each of the five walls in the RD

(realistic support – dynamic loading) test series was subjected to a unique set of 10 minute wind storms. Within each set, individual wind storms were defined such that the mean wind speed began at 14 m/s (0.13 kPa) for the first storm in the set and increased in 2 m/s increments in each successive storm until the wall failed; the strongest wall specimens failed during wind storms with a reference mean wind speed of 36 m/s (0.84 kPa). These five sets of wind storms were then re-used for the companion walls in the ID (ideal support – dynamic loading) test series.

A sample wind force time history for a storm with a mean wind speed of 16 m/s is shown in Figure 4. To avoid introducing a potentially damaging impact load at the beginning of the storm, an initial 120 s period was used to slowly bring the applied load up to the mean value of the load time history; a further 30 s was used to transition from static to dynamic loading through the use of a linearly increasing filter applied to the turbulent load fluctuations.

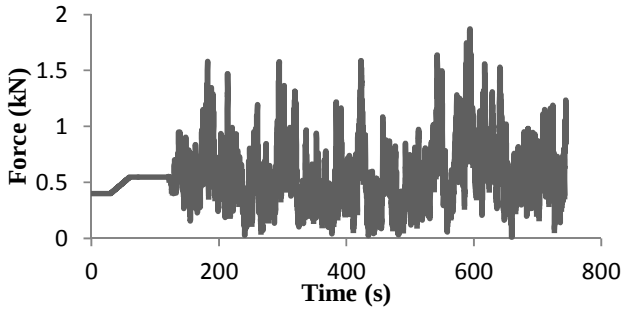

Figure 4: Sample force time history for a 16 m/s mean wind speed

Figure 5 presents a sample Power Spectral Density (PSD) plot, showing how the energy in the turbulent wind force was distributed with frequency; in this case, data is shown for the second specimen in the RD series (RD2) for a wind storm that occurred prior to cracking of the wall (16 m/s mean wind speed). This PSD plot has been normalized by the calculated variance of the force time history so that the area enclosed by the PSD is unity. In addition to the measured (applied) wind force, Figure 5 also includes PSD plots for the target simulated force (set-point), as well as for the theoretical wind spectrum on which the simulations were based (the so-called Davenport spectrum adopted by [4]). It is apparent that there is good agreement between the measured and target power spectra, particularly in the lower frequency range. This was found to be typical for the dynamic wall tests in that, prior to wall cracking, the applied load data was able to reproduce the set-point (target) quite accurately, with only small errors observed in reaching some instantaneous peaks.

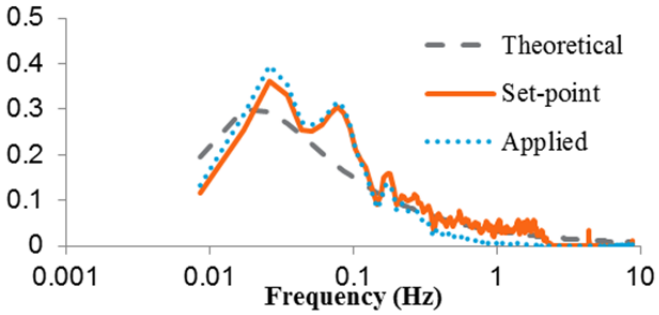

Figure 5: Force PSD plot for test wall RD2 prior to cracking (16 m/s mean wind speed)

After first cracking of the dynamic wall specimens, however, the similarity between the target and measured load histories deteriorated. As the lateral stiffness of the post-cracking walls decreased, it became increasingly difficult for the hydraulic actuator to achieve the desired load fluctuations. This behaviour is illustrated in Figure 6, which compares the target and measured load histories for wall specimen RD3, both before and after cracking (at an elapsed time of approximately 375 s) during a wind storm characterized by a nominal mean wind speed of 20 m/s (0.26 kPa). While the two plots are nearly coincident prior to cracking, it is apparent that the measured force continues to follow the general trends in the target force time history after cracking, but does not reach the desired peak vales. At higher load levels when the walls were more severely cracked, and thus even more compliant, the load control feedback mechanism became somewhat unstable, resulting in a noticeable "chattering" behaviour as the actuator attempted unsuccessfully to find the target load level; this chattering was manifest in spurious high frequency load fluctuations that occurred at a frequency of approximately 5 Hz.

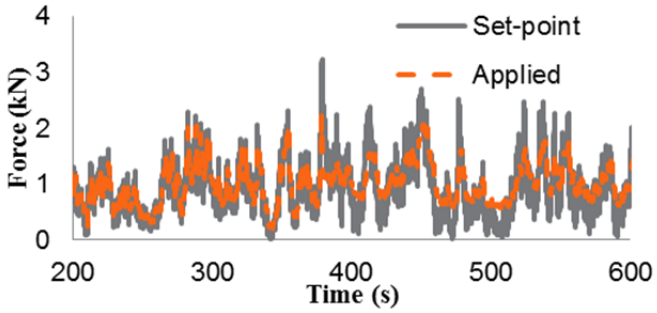

Figure 6: Sample force time history of wall RD3 before and after cracking

SUMMARY OF TEST RESULTS

Plots of the load-displacement response of static wall test specimens are shown in Figure 7; Figure 7(a) shows the plots for the ideally-pinned walls (series IS), while Figure 7(b) shows the results for the realistic wall supports (series RS). It should be noted that the displacement data for the lower displacement ranges on these plots were obtained from the LVDT's positioned at mid-height of the wall, while that for the larger displacements has been extrapolated from the LVDT attached to the hydraulic actuator since the LVDTs measuring wall displacements were removed prior to collapse to avoid damage to the instrumentation.

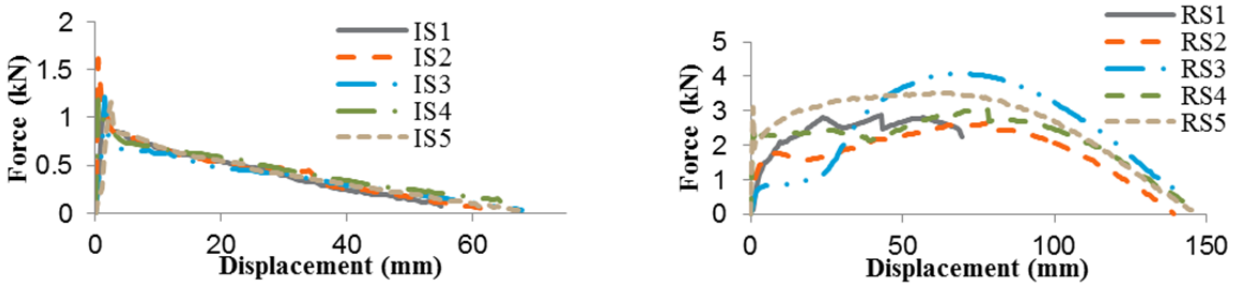

Figure 7: Load-displacement plots for static load tests: (a) ideal supports (IS) and (b) realistic supports (RS).

As shown in Figure 7(a), the static loading response for the five ideal support specimens (series IS) was very consistent. A horizontal crack occurred along a mortar joint near mid-height at a small lateral displacement, followed by a rapid drop-off in load-carrying capacity, then a gradual, nearly linear reduction in load resistance with increasing displacement until collapse.

The load-deflection plots of the realistic support specimens (Figure 7(b)), on the other hand, exhibited more variability, although the sequence of failure was consistent, with the first crack appearing near mid-height, followed by a second crack along the bed joint either immediately below or above the lowest course of blocks, and finally a third crack forming below the top course that gave rise to an unstable mechanism leading to collapse of the wall. Of the five specimens in the RS series, only walls RS4 and RS5 exhibited distinct first cracking peaks similar to the IS specimens. It should be noted, however, that the load spreader system for specimen RS1 (the first specimen tested) did not perform as intended, leading to an uneven distribution of loading between the two loading levels on the wall; this problem was rectified in subsequent tests. In addition, specimen RS3 was loaded past cracking, unloaded and then reloaded, leading to the different response pattern for that wall. Nevertheless, the post-cracking behaviour of the RS specimens was remarkably similar, with substantial post-cracking gains in lateral load resisting capacity and large lateral displacements prior to collapse. The post-cracking strengthening of the RS walls can be attributed to the clamping action of the top support angles, which induced both a restraining moment and a compressive axial force due to prying behaviour as the wall attempted to rotate at its top end. It should be noted that this end restraint resistance is partially dependent on the stiffness of the guide angle supports, which in this case were more closely spaced than would normally be the case in practice due to the limited width of the specimens. The typical deflected shape of the RS specimens near collapse is shown in Figure 8, clearly illustrating the bi-linear collapse mechanism and large lateral displacement that was achieved under displacement controlled loading conditions.

Figure 8: Deflected shape of realistically supported wall (series RS) near collapse

A summary of the lateral mid-height displacements of all wall specimens at various loading stages is presented in Table 1, including displacements at first cracking, at the ultimate load (defined as being the highest load attained during the static loading time history, or as the peak load at the initiation of complete failure of the wall in the dynamic tests) and at the instant of collapse. Since the maximum load for the ideal support specimens (series IS and ID) was observed at first cracking, the ultimate and first cracking loading stages occurred simultaneously for those specimens.

Table 1: Lateral displacements at wall mid-height

Loading Stage	Test Series	Mean (mm)	Max. (mm)	Min. (mm)	C.O.V. (%)
1st Cracking	IS	0.36	0.43	0.25	19.1
	ID	0.30	0.52	0.16	51.4
	RS	0.89	1.64	0.23	79.7
	RD	0.96	1.25	0.25	42.9
Ultimate	RS	73.92	86.70	61.55	14.7
	RD	91.62	94.77	86.99	3.6
Collapse	IS	66.80	75.47	60.51	10.0
	ID	60.74	70.46	51.60	13.6
	RS	147.21	165.40	139.30	7.2
	RD	151.86	172.84	140.73	8.3

The mid-height displacements at first cracking were typically less than 1 mm for all wall specimens, although there was considerable variability in this value; first cracking data for two of the RS series specimens were excluded from Table 1 since they were deemed to be suspect, in addition ultimate displacement for RS1 was removed. It is apparent that the realistically supported specimens (series RS and RD) sustained substantial lateral displacements, averaging 83 mm and 150 mm at ultimate and collapse conditions, respectively. In addition, the average displacement at collapse of the realistic specimens was found to be twice as large as that for the ideal support specimens (series IS and ID). Defining the apparent “ductility” of the walls as the mid-height displacement at ultimate conditions divided by that at first cracking, the average ductility for the realistically supported walls was found to be 89, on average, compared to a ductility of unity for the ideally pinned walls.

Considering only the realistic support series, the dynamically loaded specimens (RD) attained approximately 24% higher displacements at ultimate, however, collapse occurred at a similar displacement as the statically loaded specimens (RS), on average. It appeared that collapse was initiated in all specimens when a geometrically unstable displaced configuration was reached, as suggested in Figure 8, regardless of loading type.

Calculated bending moments at mid-height of the walls are presented in Table 2 for the first cracking and ultimate loading stages. These bending moments were estimated based on the four point loading arrangement, assuming simple spans for all the walls. Since the ideal support specimens were 76.2 mm (3 in) taller than the realistic specimens due to the location of the

pinned connections on the supports, the calculated moments are also presented in a normalized form in Table 2; here, the normalized moment is defined as the calculated moment divided by the theoretical first cracking moment of the wall (1.05 kN-m and 1.14 kN-m for the ideal and realistic walls, respectively), assuming linear behaviour and a specified tensile strength of $f_t = 0.40$ MPa [10].

Table 2: Calculated mid-height bending moments

Loading Stage	Test Series	Filter cut-off	Mean (kN·m)	Max. (kN·m)	Min. (kN·m)	C.O.V. (%)	Normalized Moment
1st Cracking	IS	-	0.69	0.71	0.66	3.4	0.65
	ID	-	0.76	0.85	0.69	8.5	0.72
		1 Hz	0.71	0.80	0.68	8.2	0.68
	RS	-	1.34	1.69	0.92	29.2	1.17
	RD	-	1.19	1.40	1.00	12.0	1.05
		1 Hz	1.08	1.30	0.95	13.2	0.95
Ultimate	RS	-	1.77	2.26	1.45	18.1	1.55
	RD	-	1.98	2.36	1.62	14.2	1.74
		1 Hz	1.40	2.01	1.01	26.5	1.23

Comparing the normalized moments at ultimate conditions, the realistic support (RS) samples exhibited a 139% increase in moment capacity under static loading as compared to the ideal (IS) samples, on average, while the dynamically loaded RD wall specimens showed an average increase of 142% over the ID specimens. Regardless of loading type, therefore, the realistic supports led to a significant increase in moment capacity as compared to the idealized supports.

The influence of the loading type on moment capacity was less clear. For wall specimens featuring ideal pinned supports, the dynamically loaded specimens (ID) sustained 10.8% higher moments at ultimate loading (which was coincident with first cracking), on average, than the statically loaded walls (IS). For the realistic support condition, on the other hand, the dynamically loaded walls sustained an average of 10.3% lower moments as compared to the static specimens. These differences were tested to not be statistically significant, given the observed levels of variability in the test results. It should be noted, though, that the dynamically loaded specimens were tested under load control, where the actuator control system was set to reproduce target instantaneous load levels regardless of the required displacements, while the statically loaded specimens were tested under displacement control where the enforced wall deformations occurred in a much more gradual and less violent manner. In addition, the dynamically loaded walls were incrementally damaged by a series of successively more intense wind storms, rather than a single, monotonically increasing load history, as was the case for the static tests.

To get a sense of how the dynamically loaded walls responded to load fluctuations of different durations, a digital low-pass filter was applied to the measured data to remove selected high frequency fluctuations. For the results discussed here, a first-order Butterworth low-pass filter, as implemented in Matlab™ [11], was chosen, using a high frequency cut-off of 1.0 Hz. A sample

plot of the filtered and unfiltered measured force time history for specimen RD1 is shown in Figure 9. As suggested by this plot, the dynamic response of severely cracked walls was found to feature high frequency fluctuations (the "chatter" mentioned previously) superimposed on more slowly changing, quasi-static response variations. As illustrated in Figure 9, the walls typically failed during longer duration periods of elevated filtered (low frequency) response (i.e. during large, sustained gusts), possibly because this allowed the walls the time required to reach the critical unstable displaced pattern required to cause collapse. Therefore, it was not necessarily the largest peak in the unfiltered load history that led to collapse, but rather it was high instantaneous peaks associated with larger sustained load fluctuations.

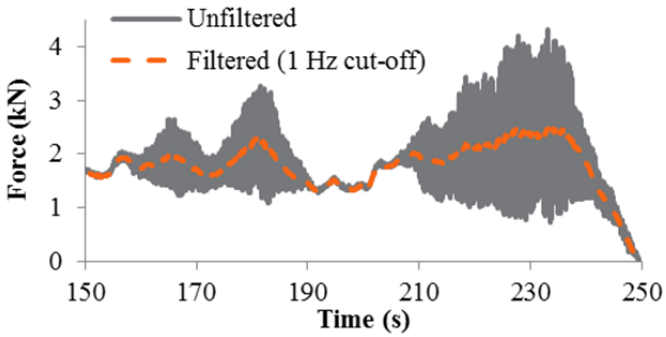

Figure 9: Filtered and unfiltered load time history of specimen RD1 near failure.

Peak bending moments at ultimate conditions calculated from the low-pass filtered dynamic force data are included in Table 2. It was found that, on average, the ultimate normalized bending moment determined from the filtered data was 94% of that from the unfiltered data for the ideal support specimens (series ID) but only 71% for the realistic support specimens (series RD). This suggests that the increased end restraint provided to the RD walls allowed them to withstand larger high frequency fluctuations without collapse. However, because the frequency content in the applied load differed for uncracked and cracked walls (due to the controller stability issues discussed previously), with more high frequency fluctuations in the severely cracked state, these results cannot be considered to be conclusive.

SUMMARY AND CONCULSIONS

A total of twenty unreinforced masonry block walls were tested under both quasi-static loading conditions and dynamic loading that simulated the natural wind. The wall specimens were constructed with supports that either approximated ideal pinned connections or were similar to more realistic, nominally "pinned" supports commonly encountered in practice.

The walls featuring "realistic" supports exhibited lateral displacements at failure that were approximately twice as large as those with ideal pinned supports. In addition, the more realistic support restraint resulted in ultimate midspan bending moments that were approximately 2.4 times as large for the statically loaded walls and, similarly, 2.4 times as large for dynamically loaded specimens as compared to companion specimens with ideal pinned supports.

The influence of loading type was found to be less dramatic. While dynamically loaded specimens exhibited somewhat higher displacements both at ultimate loads and collapse (10.8% and 10.3%, respectively), failure in all cases seemed to be initiated when the wall reached a

geometrically unstable displaced shape. For realistic supports, peak bending moments in the dynamic tests were found to be slightly (12%) higher than those for companion static tests, although this difference was not statistically significant. In the dynamic tests, failure seemed to occur during a large, sustained "gust" that allowed the wall time to displace sufficiently.

Based on observations from the current test program, it seems reasonable to suggest that the difference between static and dynamic lateral loading may be more pronounced for reinforced masonry walls since post-cracking stiffness and resilience would be higher, potentially allowing the reinforced walls to better withstand short-duration, large amplitude load fluctuations.

AKNOWLEDGEMENTS
Financial support from the Saskatchewan Centre of Masonry Design, the Saskatchewan Masonry Institute, and the Natural Sciences and Engineering Research Council of Canada is gratefully acknowledged. The authors would also like to acknowledge laboratory technicians, Brennan Pokoyoway and Dale Pavier, for their valuable assistance as well as Roy Nicholas of Gracom Masonry for construction of the test specimens.

REFERENCES

[1] Griffith, M.C., Lam, N.T.K., Wilson, J.L, and Doherty, K. 2004. Experimental Investigation of Unreinforced Brick Masonry Walls in Flexure. J of Struct Engin, **130**(3): 423-432.

[2] Beak, M., Colwell, S.A., Crowhurst, D., and Ellis, B.R. 1994. The Behaviour of Masonry and Concrete Panels Under Explosion and Static Loading. Proc of I Chem E Symp Series No. 134, pp. 227-247.

[3] Van Straaten, R.A., Kopp, G.A., and Straube, J.F. 2010. Testing Water Penetration Resistance of Window Systems Exposed to "Realistic" Dynamic Air Pressures". International Conference on Building Envelope Systems and Technologies (ICBEST).

[4] NBCC. 2010. National Building Code of Canada, National Research Council of Canada, Ottawa, Canada.

[5] Liu, Y. and Hu, K. 2007. Experimental study of reinforced masonry walls subjected to combined axial load and out-of-plane bending. Can J of Civil Engin, **34**:1486-1494.

[6] Bean Popehn, J.R., Schultz, A.E., Lu, M., Stolarski, H.K. and Ojard, N.J. 2008. Influence of transverse loading on the stability of slender unreinforced masonry walls. Engineering Structures, **30**:2830–2839.

[7] CSA. 2004. Mortar and grout for unit masonry. CSA Standard A179-04, Canadian Standards Association, Mississauga, ON, Canada.

[8] Box, G., and Jenkins, G. 1976. Time Series Analysis: Forecasting and Control, Holden-Day.

[9] Sparling, B.F., and Davenport, A.G. 1998. Three dimensional dynamic response of guyed towers to wind turbulence. Can J of Civil Engin, **25**:512-525.

[10] CSA. 2004. Design of masonry structures. CSA Standard S304.1-04, Canadian Standards Association, Mississauga, ON, Canada.

[11] Mathworks. 2002. MATLAB users manual. Mathworks Inc.Massachusetts, USA.